Capacity Statistics Evaluation for Next Generation Broadband MEO Satellite Systems

Capacity Statistics Evaluation for Next Generation Broadband MEO Satellite Systems

Charilaos I. Kourogiorgas, *Student Member, IEEE*, Daniele Tarchi, Alessandro Ugolini, *Senior Member, IEEE*, Nikolaos Lyras, Pantelis-Daniel Arapoglou, Athanasios D. Panagopoulos, *Senior Member, IEEE*, Giulio Colavolpe, *Senior Member, IEEE*, Alessandro Vanelli-Coralli

***Abstract*—In this paper, the performance of a reference Medium Earth Orbit (MEO) satellite constellation system operating at Ka-band and employing single links to ground is compared with next generation advanced systems in higher RF or optical bands employing multiple diversity links. The fill rate of existing MEO constellations offering broadband and trunking services in Ka-band is growing fast rendering the seach for additional spectrum of vital importance. Therefore, this paper reports on the results of a system study investigating the option of using Q/V band instead of Ka-band, or even optical wavelengths to deliver substantially higher system capacity. The system study takes a holistic approach covering from atmospheric channel impairments to waveform optimization and system analysis for realistic assumptions. Firstly, the system characteristics and assumptions of the various reference and advanced system candidate options are presented. Then, in order to evaluate the system a sophisticated channel model is proposed which is able to generate time series of atmospheric attenuation correlated on spatial and temporal domain. Furthermore, an optimization on the performance at Physical Layer is performed to derive the necessary inputs to the system analysis (e.g. tables of modulation and coding thresholds). The system performance in terms of outage probability and outage capacity is calculated for various locations of single ground stations, multiple ground stations (site diversity) and from multiple satellites (orbital diversity technique). Five different advanced high frequency RF and optical systems are compared in terms of outage capacity and availability assuming similar on board satellite resources (mass, power), achieving a high degree of realism in the comparison.**

***Index Terms*—MEO constellation; Trunking system; Outage Capacity; Space-Time synthesizer;**

I. Introduction - ALL

The use of satellite communications for broadband and trunking services is a promising solution in regions where terrestrial backhauling, either wireless or wireline, is hard to be established, e.g. islands, or inadequate. Although, most satellite communication systems are employing Low Earth Orbit (LEO) or Geostationary Earth Orbit satellites, very recently the use of Medium Earth Orbit (MEO) satellites has shown great potential and has led to a high fill rate of the multiple satellites taking part in the constellation [1].In order to provide services quasi-globally a smaller number of MEO satellites in the constellation is needed compared to a LEO constellation. Moreover, free space losses and the latency due to propagation is smaller than in GEO links [2]. The O3b system is already operational in Ka-band and uses ten satellites in equatorial orbit [1], while other MEO systems in similar orbits are currently under investigation, even at optical wavelengths [3].

Owing to this high demand for broadband and trunking traffic from MEO, it is of interest to pursue technologically advanced solutions that can offer additional spectrum for next generation systems. One step-wise option is to migrate to a higher than Ka- frequency band (20/30 GHz), namely Q/V-band (40/50 GHz). A more disruptive approach is to consider what communication technology at optical wavelengths can offer. In Q/V band, atmospheric phenomena are harsher than in Ka-band. In particular, rain, atmospheric gases and clouds cause the attenuation of the signal, while amplitude scintillation occurs due to the turbulence in the troposphere [4]. Although, rain is the dominant fading mechanism at both Q- and Ka-bands, the atmospheric attenuation is increased compared to the attenuation at Ka-band. Therefore, the use of Fade Mitigation Techniques (FMTs) [4] must be considered.

Adaptive Coding and Modulation (ACM) is a FMT which has been already adopted in the second generation of ETSI standard for Digital Video Broadcasting on satellite links, DVB-S2 [5] and its extension DVB-S2X [6]. It is also implemented in the currently operation O3b system. However, at Q/V-band, ACM mayu not be enough to achieve the desired link availability due to atmospheric attenuation and, therefore, spatial diversity becomes necessary. Two spatial diversity architecture are of interest: a) Site diversity: in which two or more ground stations are communicating with the same satellite and b) Orbital diversity: one ground station communicates with two or more satellites. In both techniques, the links that are used for the communication between Earth and satellite are spatially separated. This spatial separation decreases the correlation of atmospheric attenuation induced in the links. The performance of MEO constellation for single links at Ka and Q-bands has been also evaluated using ACM technique for a small number of ground stations at [7] and [8], respectively.

This paper reports on a system study performed under the

This work was supported by SatNEX-IV program of European Space Agency.

C. I. Kourogiorgas, A. D. Panagopoulos are with School of Electrical and Computer Engineering, National Technical University of Athens, Iroon Polytechniou 9, Zografou- Athens (E-mail: harkour@mail.ntua.gr, th-panag@ece.ntua.gr). A. Ugolini and G. Colavolpe are with Dipartimento di Ingegneria dell'Informazione, University of Parma, Parco Area delle Scienze 181/A, I-43124 Parma, Italy (E-mail: alessandro.ugolini@unipr.it, giulio.colavolpe@unipr.it).

SatNEx IV comparing various options in next generation MEO satellite systems. Having as reference a system similar to today's O3b operating at Ka-band we investigate the benefits in terms of system capacity (equivalent throughput) of migrating to Q-band. [1] Being a more disruptive approach. we also devote a smaller part of the system study to a MEO system option employing optical wavelengths. In total, five systems with different operating frequencies and spatial techniques are considered: a) single link Ka-band, b) single link Q-band, c) site diversity at Q-band, d) orbital diversity at Q-band and e) optical wavelength. The comparison between these five system option is done to the extent possible based on equal or similar mass and power satellite payload resources.

The system study follows a holistic approach, that is it covers all necessary elements from simulating the orbit for the whole MEO constellation to providing an accurate spatio-temporal time series synthesizer as an atmospheric channel model to making an in depth waveform and physical layer optimization using a realistic satellite payload. All this is done to finally run the system level simulations using the outputs of these modeling efforts. A sophisticated channel model is developed in order to generate time series of attenuation for single link and spatially separated links reproducing the spatial and temporal behavior of atmospheric attenuation. Furthermore, being a broadband interactive system, the RF options assume adaptive coding and modulation (ACM) employing a wide range of possible modulation and coding (MODCOD) options from the DVB-S2 and DVB-S2X standards [5], [6]. The thresholds for these MODCODs are calculated based on thorough optimization of the physical layer.

The remainder of the paper is organized as follows: in Section II, the system , orbital and geometric characteristics are given. In Section III, the channel model used for the generation of the atmospheric attenuation time series is described, while in Section IV, the optimization methodology on the physical layer for the calculation of the MODCOD tables is presented. In Section V-C, numerical results on the capacity statistics are presented and the different systems are compared in terms of availability and offered capacity.

II. MEO System Definition and Characteristics

In order to fairly compare the various system options, a number of common system limitations are adopted. Firstly, it is assumed that the DC power consumption on-board the satellite payload must be equal to 1300 W, the system must at least provide a target availability of 99.9% and a total propagation latency constraint for the complete forward link (gateway, satellite, user terminal) has been set to 150 ms. The latter limitation has been set in order to design a system which could be used to provide delay intolerant service, which is a MEO stronghold. Finally, as the Ka- and Q-band systems use both the same antenna sizes and the same frequency re-use across their spot beams, the mass of the satellite payload also turns out similar.

[1] As our study is limited to the satellite to user terminal downlink, we only refer to Q-band in the following.

TABLE I: Chosen Ground Stations

Location	Latitude (deg)	Longitude (deg)
Nemea, Greece	37.8^o	22.65^o
Lima, Peru	-12.04^o	-77.04^o
Hawaii, US	19.74^o	-155.65^o
Dubbo, Australia	-32.25^o	148.61^o
Vernon, Texas, US	34.15^o	-99.30^o
Karachi, Pakistan	24.96^o	67.06^o
Sintra, Portugal	38.8^o	-9.38^o
Hortolandia, Brazil	-22.97^o	-47.21^o

In order to properly assess the available system spectrum an analysis of the spectrum limitations in the Q-band has been performed by taking into account the ITU-R Radio Regulations (in particular Article 5) [9]. It is found from [9] that the frequency interval between 37.5 GHz and 42.5 GHz belonging to the fixed satellite service could be used even if it can be also allocated to high-density applications. Therefore, for every satellite an available bandwidth of 5 GHz is assumed.

The constellation considered consists of 8 MEO satellite with equal spacing, i.e. 45^o. Each satellite has an altitude of 8062 km above mean sea level and an inclination angle of less than 0.1^o. Each satellite has 12 steerable antennas, 10 of which are used for the user beams while 2 of them are used for the gateways. The antenna efficiency is 65% and the diameter is equal to approximately 22 cm. Each steerable antenna creates a single spot beam on ground and is fed by a unique transponder. As mentioned, between the Ka- and Q-band systems we assumed the same frequency re-use factor equal to two. In turn this means that each transponder (beam) in the Q-band system, reusing the 5 GHz twice per satellite, will occupy per transponder. The term transponder should be understood as a payload chain with a single Traveling Wave Tube Amplifier (TWTA) with a saturated RF power of 65 W with a 50% efficiency. This value keeps the total DC power consumption of the 10 user beams at the level of 1300 W.

To capture the variability of climatic conditions and corresponding propagation effects, seven (7) ground station location are assumed for the user links. The chosen stations as well as their locations are shown in Table I. [2] Two classes of user terminal antennas will be used: 1.8 m and 3.5 m (the antenna efficiency is 65%). The global picture of the MEO constellation as well as the selected ground stations are depicted in Fig. 1. In the same figure, the contour line for the 5^o elevation angle is shown for each satellite to highlight the latitude of the possible satellite coverage.

Moreover, it is assumed that every ground station is equipped with two antennas.This is a typical operating condition in existing MEO systems as it allows for a seamless satellite handover, since one of the antennas targets the rising satellite and the other one the descending satellite. The ground station is assumed to always receive data from the satellite at the highest elevation angle.

The geometry of an orbital (satellite) diversity architecture is shown in Fig. 2. The separation angle between the two links is denoted as $\Delta\psi$ and the links may have different elevation

[2] The chosen locations are the ones also chosen from O3b for the installation of the gateways.

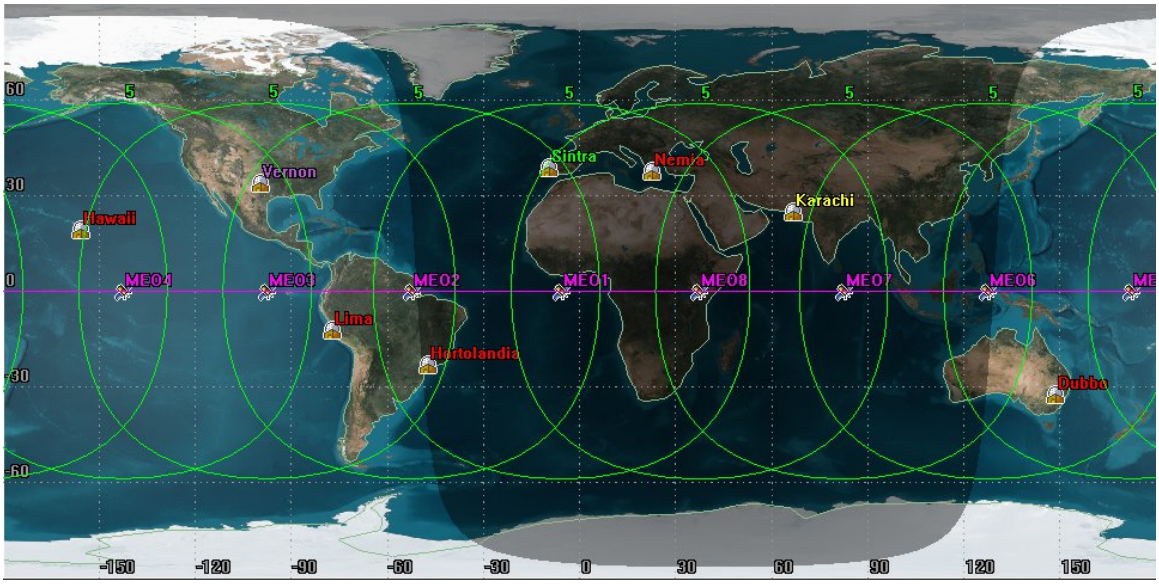

Fig. 1: MEO constellation and selected ground stations for system studies

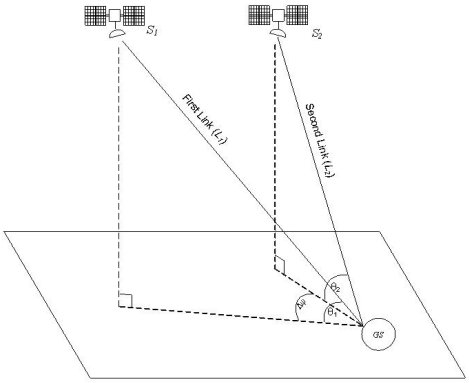

Fig. 2: System Geometry for the Orbital Diversity System

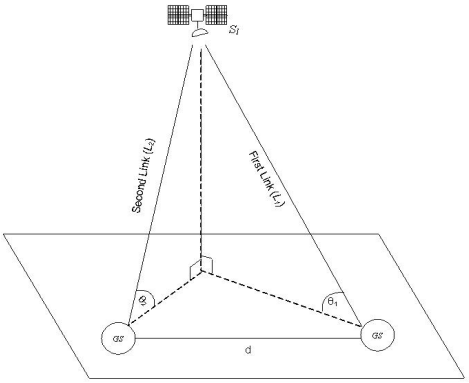

Fig. 3: System Geometry for site diversity system

angles toward the different satellites. Due to the fact that every ground station is equipped with two antennas, orbital diversity is possible in case both rising and descending satellites are transmitting the same signal to the user. Of course, this implies that a neighbouring satellite has such capacity to spare. For the choice of which link shall be used, the ground station is communicating using the link with the highest Signal-to-Noise Ratio (SNR) suffering from minimum attenuation.

For the site diversity system, two ground stations separated by a distance d communicate with a single satellite (Fig. 3). The two links are assumed to be at the same elevation angle. Therefore, each ground station of the site diversity system has two antennas and the data are delivered to Earth through the satellite seen at the highest elevation angle. The ground station with the least attenuation is chosen for the data delivery.

Turning next to the case of an optical MEO system, in line with the state-of-the-art we assume that an optical terminal on board the satellite consumes 160 W of DC power [10]. Then, to preserve the power envelope of 1300 W, on board each satellite 8 optical terminals are embarked. Current state-of-the-art of these terminals achieves a data rate per of about 5.6 Gbps [10]. Looking to the next generation of MEO systems in the mid-term, we extrapolate this data rate to 20 Gbps, assuming e.g. a spectrally more efficient modulation or the possibility for WDM (wavelength division multiplexing).

III. Channel Model

In order to evaluate system performance for diversity systems, a space-time synthesizer of atmospheric attenuation is developed, which is able to capture the spatial and temporal behavior of the medium. Total atmospheric attenuation A_{atm} time series are calculated summing up the time series of the effects of each factor [11]:

$$A_{atm}(t) = A_{rain}(t) + A_{cl}(t) + A_{wv}(t) + A_{oxygen}(t) + S(t) \quad (1)$$

where A_{rain}, A_{cl}, A_{wv}, A_{oxygen} and S are the rain attenuation, cloud attenuation, attenuation due to water vapor, oxygen attenuation, and scintillation, respectively. Here it shall be noted that, although ITU-R Recommendation P.1853 [11] provides a methodology for generating atmospheric attenuation for GEO links, it is not directly applicable to the dynamic MEO links studied in this paper.

A. Rain Attenuation

First, rain attenuation is generated using the extension of methodology in proposed in [12], [13] to take into account the time-dependence of elevation angles and the correlation between the spatially separated links for orbital and site diversity. The synthesizer assumes that for a given elevation angle (θ), rain attenuation is considered as a lognormal distribution with median value $A_m(\theta)$ and $S_A(\theta)$. However, due to the MEO satellite orbital characteristics, the synthesizer considers the time dependency of the statistical parameters (A_m and S_A) of the lognormal distribution of rain attenuation and the temporal evolution of the dynamic parameter (β) of rain attenuation (for detailed explanation see [12] and [13]). Now, considering n spatially separated links, rain attenuation induced on link i is denoted as $A_{rain,i}$. For the generation of rain attenuation time series, the time series of the Gaussian process (U_i) are generated for every link using the following multidimensional Stochastic Differential Equation (SDE) [14], [15]:

$$\mathbf{U}_t = e^{\int_0^t \mathbf{B}_y dy}\mathbf{U}_0 + e^{\int_0^t \mathbf{B}_y dy}\int_0^t \exp\left(-\int_0^y \mathbf{B}_{y'}dy'\right)\mathbf{S}_y d\mathbf{W}_y \tag{2}$$

where $\mathbf{B_t}$ is a $n \times n$ matrix with elements $b_{ij,t} = -\beta_{i,t}\delta_{ij}$ with δ_{ij} the Kroenecker delta function and $-\beta_{i,t}$ the dynamic parameter of rain attenuation as defined in [16]. The matrix $\mathbf{B}$ is time dependent since, as shown in [12], its elements depend on the elevation angle and therefore for MEO slant paths, the dynamic parameter is time dependent.

Continuing from (2), $\mathbf{W_t}$ is the n-dimensional Brownian Motion, [15]. From [17], the matrix $\mathbf{S}$ is calculated from the Cholesky decomposition of matrix $\mathbf{G_U}$:

$$[G]_{ij} = (\beta_i + \beta_j)\,[C_U]_{ij} \tag{3}$$

where β_i and β_j are the dynamic parameters of rain attenuation for the links i and j and the $n \times n$ matrix $\mathbf{C_U}$ is the covariance matrix of the process U:

$$\mathbf{C}_U = \begin{pmatrix} 1 & \cdots & \rho_{1n} \\ \vdots & \ddots & \vdots \\ \rho_{1n} & \cdots & 1 \end{pmatrix} \tag{4}$$

where ρ_{ij} is the correlation between processes U_i and U_j. Differently than for GEO, in MEO slant paths matrix $\mathbf{S}$ in (2) is time dependent. However, there is a difference in the correlation coefficient ρ between the orbital diversity and site diversity scenario. In site diversity, the correlation coefficient proposed by Paraboni-Barbaliscia, also adopted by ITU-R. P. 618 [18] is used. This depends only on the separation distance between ground stations and remains constant over time. However, for orbital diversity, the correlation coefficient is calculated from the methodology proposed in [19]. Therefore, it depends on the elevation angle of the links and, as a result, it is time dependent.

Now, rain attenuation time series on link i, is calculated through the following transformation:

$$A_i(t) = A_{m,i}(t)\exp\left(S_{a,i}(t)U_i(t)\right) \tag{5}$$

B. Cloud Attenuation

For cloud attenuation, the methodology recommended in ITU-R. P. 1853 [11] is extended for multiple and spatially separated links. The synthesizer for attenuation due to clouds is based on generating time series of Integrated Liquid Water Content (ILWC) on a point. Then, using the recommendation of ITU-R. P. 840 [20] based on the Rayleigh approximation for scattering and absorption, the time series of attenuation due to clouds are generated from the time series of ILWC.

For the generation of ILWC time series, based on [11], the ILWC on point i is calculated through:

$$\begin{gathered} L_i(t) = \exp\left(erfc^{-1}\left(erfc\left(\tfrac{G_{C,i}(t)}{\sqrt{2}}\right)/\left(P\left(L_i > 0\right)/100\right)\right)\right. \\ \left.\cdot\sqrt{2}\cdot s + m\right),\, for\ G_{C,i}(t) > a \\ L_i(t) = 0\ for\ G_{C,i}(t) \leq a \end{gathered} \tag{6}$$

where s and m are the statistical parameters of ILWC, $P(L > 0)$, the probability of cloud presence on a point derived from ITU-R. P. 840 [20]. Furthermore, α is calculated from:

$$a = Q^{-1}(P(L > 0)) \tag{7}$$

where Q^{-1} is the inverse of the Gaussian-Q function. The time series of the Gaussian process $G_{C,i}$ for link i are calculated from the superposition of the Gaussian time series X_i^1 and X_i^2 using:

$$G_{C,i}\left(kT_S\right) = \gamma_1 X_i^1(kT_S) + \gamma_2 X_i^2(kT_S) \tag{8}$$

where T_S is the sampling period and the parameters γ_1, γ_2 are derived from [11]. The time series of X_i^1 and X_i^2 for the single link i are derived through passing white zero mean and unity variance Gaussian noise from two lowpass filters with cut-off frequency 7.17 x 10^{-4} sec^{-1} and 2.01 x 10^{-5} sec^{-1}, respectively. In order to extend the above mentioned methodology to multiple links, multi-dimensional correlated Gaussian noise is used. To include the spatial correlation, the n-dimensional noise is multiplied with the correlation matrix:

$$\mathbf{C}_X = \begin{pmatrix} 1 & \cdots & \rho_{C,1n} \\ \vdots & \ddots & \vdots \\ \rho_{C,1n} & \cdots & 1 \end{pmatrix} \tag{9}$$

where $\rho_{C,ij}$ si the correlation coefficient for the Gaussian processes between the link i and j. For the correlation coefficient the formula proposed in [21] as a function of separation distance (d) is used:

$$\rho_C(d) = 0.35\, e^{-\frac{d}{7.8}} + 0.65\, e^{-\frac{d}{225.3}} \tag{10}$$

Therefore, in case of site diversity the correlation coefficient is constant with constant separation angle. For the orbital diversity scenario, the separation distance is set equal to the distance between the two converging links at the low cloud base, which is set equal to 1 km a.m.s.l. [21]. So, the correlation matrix is time dependent for the orbital diversity scenario.

C. Attenuation due to Atmospheric Gases

Attenuation also occurs due to water vapor and oxygen molecules. Similarly to cloud attenuation, the ITU-R. P. 1853 is implemented for generating time series of attenuation on a single link. However, the attenuation time series must be correlated also in the spatial domain, since spatial diversity techniques are used.

Oxygen attenuation on a link with constant elevation angle is considered constant over time. Moreover, the same oxygen attenuation value is considered for the spatially separated links, due to the very high spatial correlation that oxygen distribution exhibits [22]. Therefore, attenuation due to oxygen is calculated using ITU-R. P. 676 recommendation [23] at a specific exceedance probability. The same value is used for all the spatially separated links with the same elevation angle. However, in case of MEO the oxygen attenuation changes over time, since the elevation angle of the link changes also.

The methodology for generating attenuation due to water vapor on multiple links is the extension of the methodology presented in [11]. According to ITU-R. P. 1853, firstly, the time series of Integrated Water Vapor Content (IWVC) are generated for a single point and then using ITU-R. P. 676 [23] the attenuation due to water vapor time series induced in a single link are calculated.

The IWVC on a single point i is considered as a stochastic process following the Weibull distribution [24], with statistical parameters λ and κ. The time series of IWVC on point i are generated through:

$$IWVC_{i,t} = \lambda(-\ln\left(Q\left(Y_{i,t}\right)\right))^{1/\kappa} \tag{11}$$

where $Y_{i,t}$ are generated from lowpass filtering of zero mean unity variance white Gaussian noise. The low-pass filter is considered with a cut-off frequency of $3.24x10^{-6}sec^{-1}$. In order to extend the methodology for n multiple links, n low pass filters are used and the n-dimensional input Gaussian noise is correlated. The correlation coefficient is derived from [22]. The correlation coefficient depends on the separation distance between the links. For the case of site diversity this distance is equal to the distance between the ground stations, while for orbital diversity the separation distance is the distance between the links at a height of 1 km a.m.s.l.

D. Scintillation

The last factor that must be taken into account is the scintillation effects. Amplitude scintillation time series are generated through the modification of the methodology presented in [25]. In the latter model, stochastic differential equations driven by fractional brownian motion are used in order to generate time series following a Gaussian distribution with a lowpass power spectrum with a slope of -80/3 dB/decade. The methodology of [25] similarly to [12] is modified to take into account the time dependent elevation angle. Considering the spatial correlation of scintillation, we consider this factor between spatially separated links as uncorrelated.

IV. Physical Layer Performance

In this section, we address the physical layer optimization of our system study to develop the necessary inputs for the system capacity simulation. In terms of physical layer techniques, we employ advanced distortion mitigation techniques at the transmitter and at the receiver. Despite their sophistication, the employed techniques are within the reach of current processing technology. To reflect the system scenario that is being considered for the Q-band system, the overall available transponder bandwidth of 833 MHz is split in two carriers for technology reasons (otherwise the sampling rate is considered overwhelming). Hence, we consider a scenario with two carriers per transponder (beam), and, in accordance with DVB-S2(x), we adopt phase shift keying (PSK) and amplitude and phase shift keying (APSK) constellations. At the transmitter side (gateway), to mitigate the amount of non-linear distortions due to the HPA and intermodulation due to the presence of the two carriers, we adopt the advanced iterative multicarrier predistortion scheme described in [26], while at the receiver a sufficient statistic for detection is extracted from the received signal by using oversampling at the output of a proper front-end filter [27]. For each carrier, a fractionally-spaced minimum mean-square error equalizer acts as an adaptive filter, allowing the receiver to be completely independent from a specific channel model [28]. The equalizers' training is performed in the presence of the adjacent signal in such a way that they can reject part of the interference. At this point, two alternative detection schemes can be envisaged:

1) Each of the two carriers is detected by means of a single-user detector (SUD). This represents the simplest solution from the point of view of the receiver complexity. We adopt a symbol-by-symbol SUD, which does not take into account the channel memory; this is because, in a multicarrier scenario, the main impairment is the interference from the adjacent channel, and not the memory effects introduced by the channel. This choice will allow us to evaluate the performance of the detection scheme also for high-order constellations.
2) Both carriers are jointly detected with a multiuser detector (MUD). This solution is expected to better cope with the interchannel interference, at the price of an increased complexity of the receiver [29]. To further increase the performance, we will use a MUD that takes into account one sample of the channel memory. To determine the target channel response for the detector, we will resort to an adaptive channel shortening filter [30], which processes the output of the equalizers and computes the optimal channel response for a given length (one in this case) of the interference to be considered by the detector. Due to the higher complexity of this receiver scheme, we will limit the analysis to lower-order constellations.

The adopted transponder model is that foreseen by the DVB-S2 standard [5], composed of an input multiplexer (IMUX) filter, which has the purpose of removing adjacent channels, a high power amplifier (HPA), and an output multiplexer (OMUX) filter, which reduces the spectral broadening caused by the nonlinear amplifier. The signal is further corrupted in

the downlink by an additive white Gaussian noise process with one-sided power spectral density N_0.

In the described scenario, we will evaluate the spectral efficiency (SE) achieved by the practical low-density parity-check (LDPC) codes foreseen by the DVB-S2(x) standards [5], [6]. The SE is defined as

$$\mathrm{SE} = \frac{r \log_2 M}{TB} \quad [\mathrm{bit/s/Hz}]\,, \tag{12}$$

where r is the rate of the adopted binary code, M is the cardinality of the adopted constellation, T is the symbol interval, and $B = 833$ MHz is the -3 dB bandwidth of the OMUX filter. The SE is computed with reference to a target packet error rate of 10^{-3} and it is represented in the Shannon plane as a function of P_{sat}/N, where P_{sat} is the saturation power of the HPA, and $N = N_0 B$ is the noise power in the considered bandwidth. An alternative figure of merit, useful to evaluate the performance of practical codes, is the achievable spectral efficiency (ASE), which represents the maximum SE that can be achieved by any practical MODCOD employing joint detection and decoding. It can thus be computed with no reference to a practical coding scheme. The ASE is defined as

$$\mathrm{ASE} = \frac{I_R}{TB} \quad [\mathrm{bit/s/Hz}]\,, \tag{13}$$

where I_R is the achievable information rate, which, for a system with memory, can be computed by means of the Monte Carlo method described in [31].

The aim of this section is to optimize the transmission parameters (i.e., the symbol rate, the frequency spacing between the two carriers, and the back-off of the HPA) of the described system to maximize the ASE with the two receiver structures under consideration. The MODCODs that result from this optimization are then used as input into the system level simulations. Fig. 4 reports the ASE for modulation formats with cardinality ranging from 2 to 64, with and without the use of the predistortion algorithm (*pred.* and *no pred.* curves, respectively), using the SUD receiver architecture. We point out that these curves are fully optimized, meaning that, for each value of P_{sat}/N, a different value of symbol rate and frequency spacing is selected. However, in a scenario in which we are constrained to adopt a unique symbol rate, we can resort to the practical solution of fixing a single parameters configuration. This solution is not optimal from the theoretical point of view, but we see from the black curve in Fig. 4 that the losses with respect to the fully optimized curve are very limited. This configuration corresponds to a symbol rate of 427.46 Mbaud and frequency spacing 449.38 MHz, i.e., the values optimized for an intermediate value of P_{sat}/N. Moreover, we have computed the SE achieved by several practical MODCODs with these parameters, also reported in Fig. 4. We see that the almost all MODCODs are in the range $1 - 1.5$ dB from the theoretical ASE. The details of some of the selected MODCODs are reported in Table II, where E_{s} is the average energy per symbol, and OBO is the output back-off of the HPA. The number in the first column will be used to identify the MODCODs in the next sections.

Finally, we evaluate the performance of the MUD in the considered scenario. As mentioned, for complexity reasons,

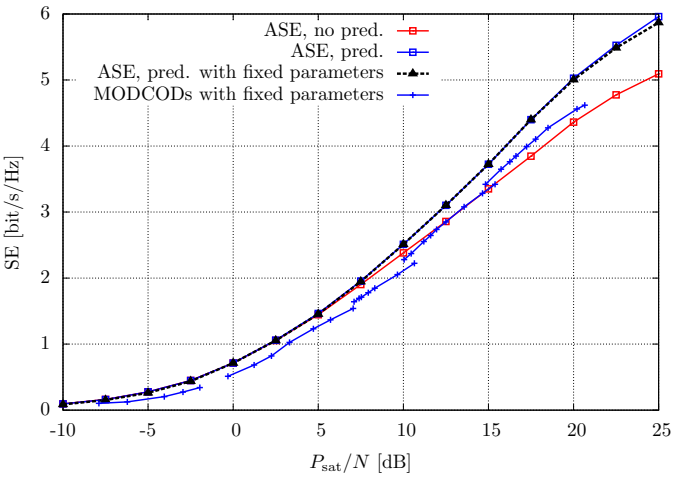

Fig. 4: Performance comparison with and without the predistorter and MODCODs spectral efficiency, using the SUD receiver structure.

TABLE II: Details of the selected MODCODs

#	Mod.	Rate	E_{s}/N_0 [dB]	P_{sat}/N [dB]	SE [bit/s/Hz]	OBO [dB]
15	8PSK	100/180	6.36	7.53	1.7105	1.06
16	8PSK	104/180	6.77	7.94	1.7789	1.06
17	8PSK	3/5	7.13	8.32	1.8474	1.08
18	8PSK	2/3	7.97	9.65	2.0526	1.57
19	8PSK	13/18	8.97	10.65	2.2237	1.57
20	16APSK	100/180	8.22	10.05	2.2807	1.72
21	16APSK	104/180	8.63	10.46	2.3719	1.72
22	16APSK	28/45	9.37	11.2	2.5544	1.72
23	16APSK	116/180	9.77	11.6	2.6456	1.72
24	16APSK	2/3	10.12	11.95	2.7368	1.72
25	16APSK	25/36	10.59	12.5	2.8509	1.8
26	16APSK	3/4	11.66	13.57	3.0789	1.8

we limit the analysis to constellations up to 16APSK. Fig. 5 compares the ASE of the MUD with that of the SUD, with and without the use of the predistortion algorithm. The optimized parameters for the MUD are reported in Table III. We see that the SUD and the MUD have a similar performance in the medium SNR range, while the MUD allows to adopt significantly higher symbol rate values at high SNR. Higher ASE values could be achieved with the MUD by transmitting completely overlapped signals with bandwidth comparable with that of the OMUX filter. However, this would lead to an excessively high sampling rate, which is not feasible for the current technology. Moreover, we have to mention that standard DVB-S2(X) LDPC codes are not designed to work together with a MUD, and they would lead to poor performance in this scenario. To fully exploit the characteristics of the MUD, a new code design is required [32]. Also in this case, we report the ASE for a practical case in which the transmission parameters have been fixed to an intermediate value. We see how this choice is practically optimal in the medium-low SNR region, while it causes significant losses at high SNR. This is due to the fact that, as mentioned, the MUD allows using higher values of symbol rate and frequency spacing, and hence a single choice of the parameters does not allow covering the whole SNR range. The selected parameters

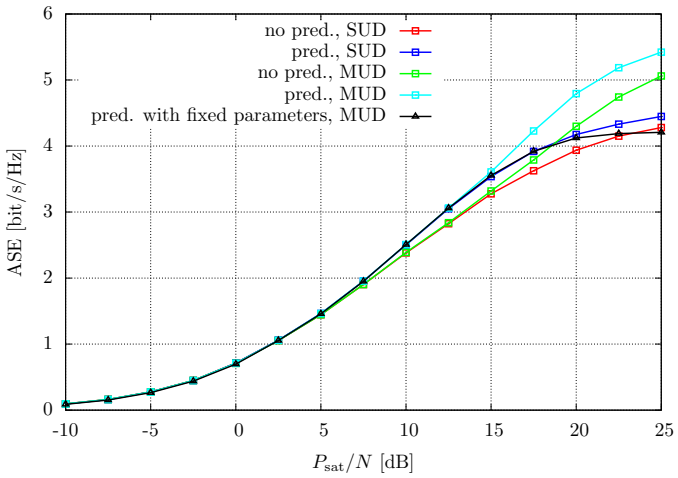

Fig. 5: ASE comparison with and without the predistorter and using the MUD receiver structure.

TABLE III: Optimized parameters for system adopting the predistorter and the MUD

Mod.	E_s/N_0 [dB]	P_{sat}/N [dB]	ASE [bit/s/Hz]	Symb. rate [Mbaud]	Freq. sp. [MHz]	OBO [dB]
8PSK	-10.94	-10.0	0.0946	416.50	405.54	0.94
8PSK	-5.82	-5.0	0.2743	405.54	405.54	0.94
8PSK	-1.05	0.0	0.7091	427.46	427.46	0.94
8PSK	3.87	5.0	1.4636	427.46	427.46	1.02
16APSK	8.09	10.0	2.5079	438.42	449.38	1.69
16APSK	11.55	15.0	3.6076	548.03	591.87	2.25
16APSK	15.29	20.0	4.7940	580.91	580.91	3.26
16APSK	18.69	25.0	5.4216	591.87	591.87	4.79

are symbol rate equal to 438.42 Mbaud and frequency spacing equal to 449.38 MHz.

V. System Simulation Results and Discussion

In this section, the simulation methodology and step-by-step algorithms are given for the calculation of capacity time series and then the required capacity statistics based on the tools developed in the previous sections. The histogram of the selected MODCODs and the outage capacity statistics are presented for the seven ground stations given in Table I.

A. Simulation Methodology

Starting with the capacity time series of the orbital diversity system operating in Q-band, the following step-by-step algorithm is used:

- At first, the time series of sub-satellite points are generated for each of the eight satellites. Toward this, the Systems Tool Kit of AGI was used [33].
- From the subsatellite points, the elevation angle from every ground station to every satellite is calculated
- For every simulation sample, the separation angle between the satellites is calculated. Then, using also as input the elevation angle time series, the correlation coefficient for every attenuation factor is calculated.
- Then, the free space losses for every sample are calculated and the channel time series are generated
- In the visibility area of the ground station the link with the least total attenuation, i.e. free space losses plus atmospheric attenuation (which follows the methodology of Section III), is selected
- For the selected link, the SNR is then calculated.
- From the SNR time series, using the MODCOD thresholds of Section IV, the capacity time series are calculated

For the site diversity scenario, we have assumed that the two ground stations are separated by 20 km and see the same satellites at the same altitude. For the generation of capacity time series, similarly to the orbital diversity after the calculation of elevation angle time series, the following step-by-step algorithm is used:

- Using the separation distance between the ground stations, the correlation coefficients for the spatial domain for all the attenuation factors are calculated
- Using the elevation angle time series and the spatial correlation coefficients, the channel time series are generated as exolained in Section III.
- The link with the minimum atmospheric attenuation is selected for the communication between Earth and space
- For the selected link, the SNR is then calculated, using the link budget parameters and the free space losses
- From the SNR time series, using the MODCOD thresholds, the capacity time series are calculated

As an illustration, in Fig. 6, the time series of elevation angle for the ground station in Hawaii are shown for the orbital diversity system. In this figure, the elevation angles for the MEO constellation is shown, when orbital diversity is used and when it is not used (only single links are possible). From the figure it is evident that the link with the highest elevation angle (single link case) does not give always the lowest attenuation.

In Fig. 7, the total attenuation, i.e. total atmospheric attenuation plus free space losses, time series are shown for the same time period as in Fig. 6 for all the links. In particular, for every sample the total attenuation in the link between the ground station and the satellites (which are visible) is shown. The same colour code of Fig. 6 is also kept in Fig. 7. SWe repeat the same type of plots for the site diversity system in Figs. 8 and 9. In Fig. 8, the black line gives the elevation angle of the system, which is the maximum elevation angle for the satellites in the visibility area of the ground stations. In Fig. 9, the atmospheric attenuation time series are shown for the site diversity system, with the black line representing the attenuation value the system is suffering from.

B. Optical Links

Going now to the optical system, the liquid water particles which are present in the cloud formations are the dominant attenuation mechanisms in optical links [21], [34]. Therefore, it is assumed that links are available only when a cloud-free environment exists. Thus, the availability of the system is equal to the probability that clouds are not present, i.e. Cloud-Free-Line-of-Sight (CFLOS) probability. For the modeling of CFLOS on multiple spatially separated links, the methodology presented in [34] is used. In this latter model, time series

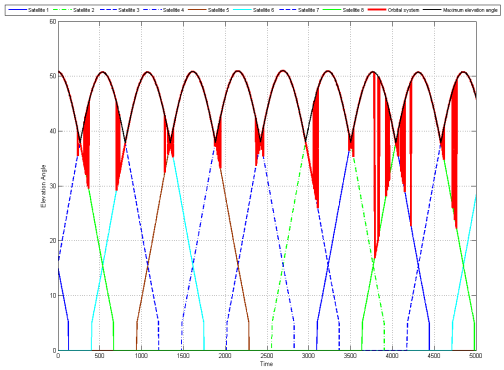

Fig. 6: Time Series of elevation angle for the orbital diversity system

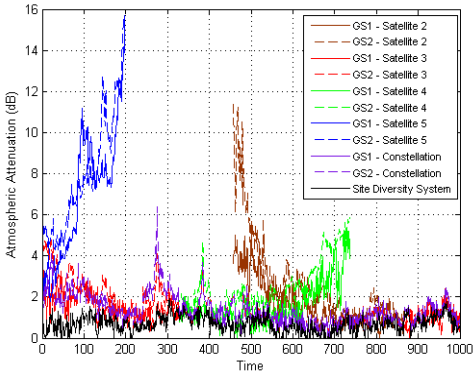

Fig. 9: Time Series of atmospheric losses for the site diversity system

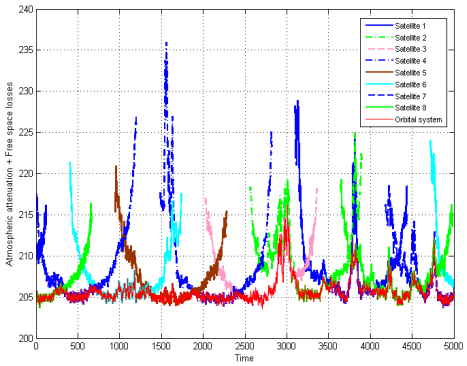

Fig. 7: Time Series of atmospheric losses and free space losses for the orbital system

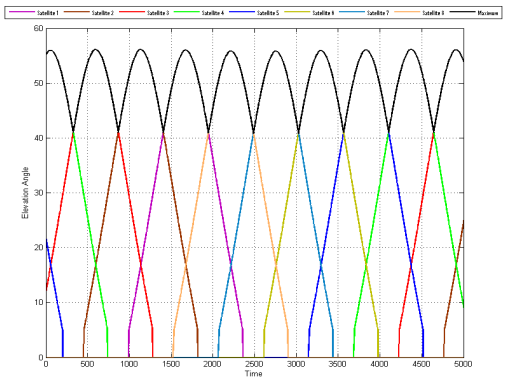

Fig. 8: Time Series of elevation angle for the site diversity system

of Integrated Liquid Water content are generated for the region of the ground station suing multi-dimensional Stochastic Differential Equations (SDEs) in order to also capture the spatial correlation of ILWC. Then, the time series of ILWC are transformed to liquid water content time series not only on the horizontal plane but also taking into account the height of each point. Therefore, after the simulation of the time series of liquid water content on three-dimension and considering the elevation angle of the link, the probability (or time percentage) that the slant path propagates through clouds can be calculated. This procedure is followed for every station of the site diversity system, taking into account through the multi-dimensional SDEs the spatial correlation of the ILWC between the stations.

The requirement that all systems under investigation must comply with is the target of 99.9% availability. This is quite a challenge for optical communications due to the deteriorating effect of clouds and spatial diversity between multiple optical ground stations at large distances is needed. To get an understanding of the number of stations required, the same set of locations in Table I has been used. For the station given in Table I, we will consider the use of spatial diversity reception in order to achieve 99.9% availability for each location.For the stations at Karachi, Vernon, and Dubbo, in order to achieve the availability target, the multiple stations were placed taking into in order to have the highest separation distance between them. For Nemea and Sintra, the number of stations required were computed using the restriction that these must be located in Greece (for Nemea) and Protugal or Spain For Sintra. Therefore, the separation distance of the stations of the site diversity was as large as the location restrictions permitted (the separation distance between two points in Greece can be close to 850 km). For Hortolandia where the probability of cloud occurrence is really high it was necessary to place several stations in different countries (like Argentina) where this probability is lower. Now for Lima we benefited from the cities in the area with high altitude and low probability of cloud occurrence.

In Table IV, the number of stations needed for every location in order to meet the target availability, i.e. CFLOS, higher than 99.9% is given. Here, it must be noted that the separation distance between the stations is mainly higher than 100 km, a fact that reveals some of the operational difficulties of setting up a high availability optical ground network.

C. Capacity Statistics

In this section, we report the numerical results from processing the capacity time series of the next generation MEO trunking system operating at Q-band; for the three different

TABLE IV: Number of ground stations considered for each region and the derived availability

Region	Number of stations	Availability [%]
Nemea	8	99.906
Karachi	5	99.94
Vernon	8	99.94
Dubbo	7	99.929
Sintra	8	99.92
Hortolandia	9	99.93
Lima	4	99.93

diversity techniques, i.e., the single link (no diversity) scenario, the orbital diversity scenario and the site diversity scenario. The single link scenario at Q-band has been studied in [8]. However, here also the results for all the stations are presented. All the system capacity results presented hereinafter assume ACM and refer to the cumulative capacity from 10 user beams per MEO satellite. Results are presented with respect to the two antenna diameters that have been considered, i.e., 1.8 m and 3.5 m, and compared with a Ka-band constellation operating with the same parameters.

The capacity results are reported for an interesting subset of those locations listed in Table I, expressed in terms of probability that capacity falls below a certain capacity threshold, expressed in bits per second (bps), in terms of probability of selecting one of the MODCOD schemes among those defined in Section IV; the first metric allows to measure the performance in terms of capacity for a target availability.

In particular in Fig. 10 the CDF of the achieved capacity is reported for the 4 selected locations (Lima, Peru - Vernon, TX, USA - Sintra, Portugal - Hortolandia, Brazil), while in Fig. 11, the probability of selecting each MODCOD schemes is reported. It is worth to be noticed that while the outage capacity figures show a comparison between the Q-band and the Ka-band systems, in case of MODCOD scheme probability of selection we report only the Q-band results; this is because the used MODCOD schemes in the two bands are different [7]. The MODCOD index refer to the index in the used MODCOD listed in Table II.

By analyzing the numerical results, it is observed that there are some dominant MODCOD schemes that are selected with a high probability during a pass of the MEO satellite over the ground station; their value depends on the location and on the antenna size but the amount of used MODCODs is quite similar in all the considered cases: almost all the used MODCODs are concentrated within a range of about 5-6 options. Moreover, it is possible to note that, while over a certain MODCOD scheme the selection probability is zero, there is a probability to select even lower values, although quite insignificant. This can be justified by the fact that there is a maximum possible MODCOD and that a selection of the lowest schemes is taking place during the very short deep attenuation intervals that occur for a small percentage of time. This is also highlighted in the Cumulative Distribution Function (CDF) of the capacity where the logarithmic scale of the CDF allows noticing that very low probability values are possible, especially for lower MODCODs.

The CDFs of Fig. 10 allow understanding the capacity

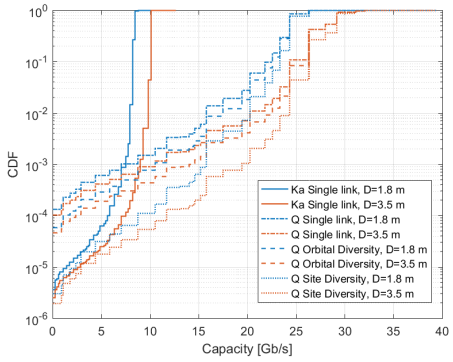

(a) Lima,Peru

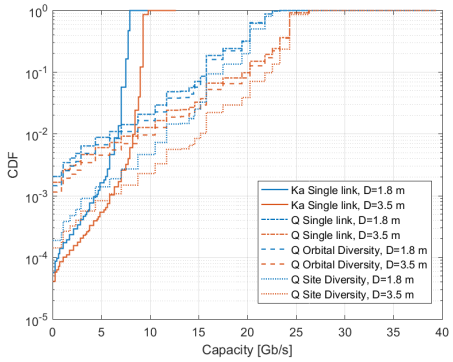

(b) Vernon, TX, USA

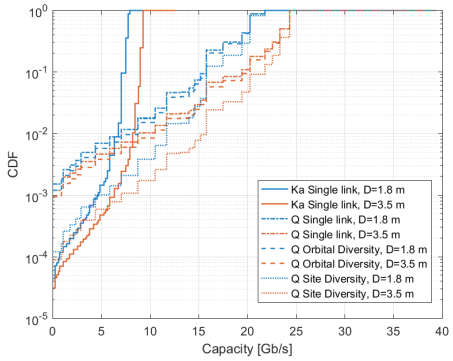

(c) Sintra,Portugal

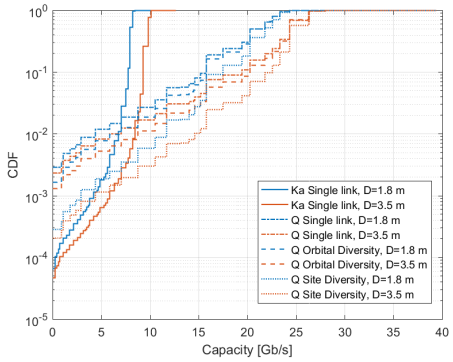

(d) Hortolandia,Brazil

Fig. 10: CDF of the capacity in the different bands and diversity schemes for the considered locations.

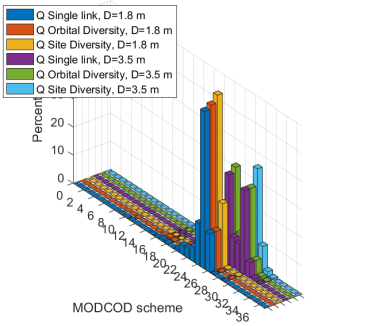

(a) Lima,Peru

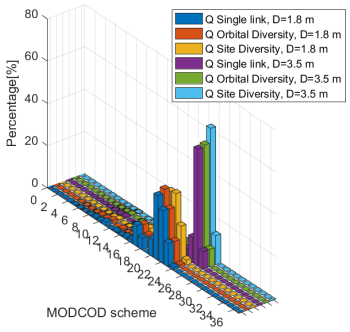

(b) Vernon, TX, USA

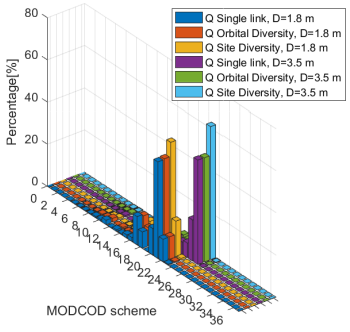

(c) Sintra,Portugal

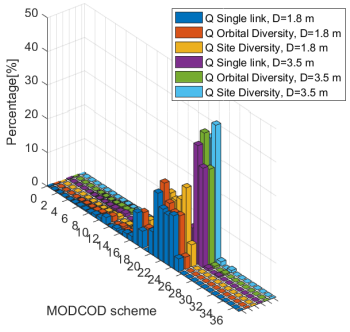

(d) Hortolandia,Brazil

Fig. 11: Histograms of the selected MODCOD schemes in the Q band in the different diversity schemes for the considered locations.

offered per MEO satellite belonging to a multi-satellite constellation by comparing the performance in Ka and Q bands. In case of Q band it is possible to achieve an impressive capacity in case of clear sky conditions corresponding to 95% availability. In this case the Q-band with single link the system achieves between 12 Gb/s in Hortolandia to 20 Gb/s in Lima for 1.8 m receiver antennas, while, in case of 3.5 m antenna, it is possible to achieve between 16 Gb/s in Vernon, Sintra and Hortolandia to 24 Gb/s in Lima. Such capacity values are about double with respect to the capacity values obtained in the Ka band for the same locations and antenna sizes. It is worth to noticing indeed that each location represent a different meteorological situation, and their difference in capacity represents the reliability of the atmospheric model previously introduced and calibrated to the different locations.

On the other side it has to be noticed that the outage probability is higher as well as the capacity for the full availability (i.e., 99.9%) is lower with respect to the Ka-band; this is due to the higher influence of the atmospheric attenuation phenomena at higher frequencies. Nevertheless, the lower capacity offered at high availability is not important due to the very limited periods that these intense phenomena occurs. What is more critical to note is that availability down to 99.9% can be preserved in Q-band even with a single station.

What is interesting instead to see is how an increased complexity at the ground side could represent remarkable advantage in terms of overall capacity. Indeed if on one side exploiting two satellites at the same time and implementing orbital diversity could slightly improve the capacity performance, it is interesting to focus the attention on the gain that can be achieved by exploiting multiple sites at the ground, i.e., implementing a site diversity. In this case, it is indeed possible to reduce remarkably the outage probability by giving nearly complete link availability to all the users.

Finally, for the capacity calculation, in order that the system of optical MEO be operational, one redundant optical terminal on board is needed for each active one. This happens because for the site diversity scheme to achieve transparent handovers without breaking the link, the alternative optical terminal needs to already have set up (pointing, acquisition and tracking) the link to a cloud free station. Therefore, since the number of terminals on the satellite is 8, we can only assume that 4 of them are active.Based on our earlier assumptions, this means that the total throughput of the optical system is 80Gbps per satellite.

VI. Conclusion

In this study various advanced options for a next generation MEO system were evaluated considering a constellation of 8 satellites and 4 possible ground station locations at different climatic areas. The outage capacity offered at 5 different scenarios was evaluated keeping satellite power consumption fixed to 1300 W, the mass similar, the latency less than 150 ms due to round trip and an availability of 99.9%. The RF ground terminals were considered with two kinds of antenna classes at 1.8 m and 3.5 m. Four RF scenarios were compared one at Ka-band (reference) and three at Q

band (advanced system) without considering any diversity, one using orbital diversity and one for site diversity. The fifth scenario considered wavelengths at optical range using the site diversity technique.

For the system design at Q-band, firstly an identification of available bandwidth at Q-band from ITU regulations was performed. It was found that 5 GHz of available bandwidth exist for satellite downlink. Since there was an available bandwidth of 5 GHz for the downlink keeping the number and size of on-board antennas the same with the Ka-band case, an 833 MHz of bandwidth at user beam was identified. Therefore, for fair comparison, the same mass on satellite and power consumption was considered. Moreover, for the system evaluation at RF, first an optimization on the PHY layer was performed to derive the ModCods at Ka and a second optimization to derive the ModCod table at Q band. More particularly, at Q band for the PHY layer two carriers were considered at each beam to reduce the noise power. For the calculation of capacity, realistic time series generator of attenuation due to atmospheric phenomena was used taking into account the spatial and temporal correlation of the attenuation factors.

From the capacity results it was found that on average there is a 100% increase in system throughput at Q/V band in comparison to reference scenario in clear sky for the same power consumption and mass on board. Moreover, in Q/V band the mean system throughput at clear sky is close to 15 Gbps for the ten user beams. However, in the single link case the 99.9% availability is not always reassured. Using orbital diversity again the 99.9% availability is not reassured for all the stations but there is an increase in both the availability and capacity. Finally, with site diversity the availability is always on target. Here it must be noted that orbital diversity can be already implemented with the existing O3b system since every ground station has already two antennas. Finally, for the optical system in most places more than 6 ground stations are required for achieving the target availability of 99.9% and close to 80Gbps can be delivered on ground.

REFERENCES

[1] O3b satellite networks. Accessed May 2014. [Online]. Available: http://www.o3bnetworks.com/o3b-advantage/our-technology

[2] S. H. Blumenthal, "Medium Earth orbit Ka-band satellite communication systems," in *MILCOM 2013 - 2013 IEEE Military Communications Conference*, Nov. 2013, pp. 273–277.

[3] Laser ligth communications. Accessed Feb 2016. [Online]. Available: http://www.laserlightcomms.com/index.php

[4] A. Panagopoulos, P.-D. M. Arapoglou, and P. Cottis, "Satellite communications at KU, KA, and V bands: Propagation impairments and mitigation techniques," *Communications Surveys Tutorials, IEEE*, vol. 6, no. 3, pp. 2–14, Third 2004.

[5] "Second generation framing structure, channel coding and modulation systems for broadcasting, interactive services, news gathering and other broadband satellite applications, part I: DVB-S2," ETSI EN 302 307-1 Digital Video Broadcasting (DVB).

[6] "Second generation framing structure, channel coding and modulation systems for broadcasting, interactive services, news gathering and other broadband satellite applications, part II: S2-extensions (DVB-S2X)," ETSI EN 302 307-2 Digital Video Broadcasting (DVB).

[7] C. Kourogiorgas, D. Tarchi, A. Ugolini, P.-D. Arapoglou, A. D. Panagopoulos, G. Colavolpe, and A. Vanelli-Corrali, "System capacity evaluation of DVB-S2X based medium earth orbit satellite network operating at ka-band," in *accepted at ASMS/SPSC Conference*, Sep. 2016.

[8] ——, "Performance evaluation of DVB-S2X based MEO satellite networks operating at Qband," in *accepted at GlobeCom 2016*, 2016.

[9] "Radio regulations - articles," ITU-R., 2012.

[10] R. Lange, F. Heine, M. Motzigemba, M. Lutzer, and R. Meyer, "Roadmap to wide band optical geo relay networks," in *MILCOM 2012 - 2012 IEEE Military Communications Conference*, Oct. 29 - Nov.1 2012.

[11] "Tropospheric attenuation time series synthesis," ITU-R. P. 1853, 2012.

[12] C. Kourogiorgas and A. Panagopoulos, "A rain attenuation stochastic dynamic model for LEO satellite systems above 10 GHz," *Vehicular Technology, IEEE Transactions on*, vol. 64, no. 2, pp. 829–834, Feb. 2015.

[13] C. Kourogiorgas, A. Panagopoulos, and P.-D. Arapoglou, "Rain attenuation time series generator for medium Earth orbit links operating at Ka band and above," in *Antennas and Propagation (EUCAP), 2014 8th European Conference on*, Apr. 2014, pp. 3506–3510.

[14] I. Karatzas and S. E. Shreve, *Brownian Motion and Stochastic Calculus*. Springer-Verlag, 2005.

[15] S. Karlin and H. Taylosr, *A second course in stochastic processes*. New York: Academic, 1981.

[16] T. Maseng and P. Bakken, "A stochastic dynamic model of rain attenuation," *Communications, IEEE Transactions on*, vol. 29, no. 5, pp. 660–669, May 1981.

[17] G. A. Karagiannis, A. D. Panagopoulos, and J. D. Kanellopoulos, "Multidimensional rain attenuation stochastic dynamic modeling application to Earth space diversity systems," *Antennas and Propagation, IEEE Transactions on*, vol. 60, no. 11, pp. 5400–5411, Nov. 2012.

[18] "Propagation data and prediction methods required for the design of Earth-space telecommunication systems," ITU-R. P. 618, 2013.

[19] J. D. Kanellopoulos, A. Panagopoulos, and S. Livieartos, "A comparison of co-polar and co-channel satellite interference prediction models with experimental results at 11.6 GHz and 20 GHz," *International Journal of Satellite Communications and Networking*, vol. 18, no. 2, pp. 107–120, 2000.

[20] "Attenuation due to clouds and fog," ITU-R. P. 840, 2013.

[21] L. Luini and C. Capsoni, "Modeling high-resolution 3-D cloud fields for earth-space communication systems," *Antennas and Propagation, IEEE Transactions on*, vol. 62, no. 10, pp. 5190–5199, Oct. 2014.

[22] N. Jeannin et al., "A space time channel model for the simulation of total attenuation fields," in *ESA Workshop on Radiowave Propagation*, Nov. 2011.

[23] "Attenuation by atmospheric gases," ITU-R. P. 676, 2012.

[24] N. Jeannin, L. Feral, H. Sauvageot, and L. Castanet, "Statistical distribution of integrated liquid water and water vapor content from meteorological reanalysis," *Antennas and Propagation, IEEE Transactions on*, vol. 56, no. 10, pp. 3350–3355, Oct. 2008.

[25] C. Kourogiorgas and A. D. Panagopoulos, "A tropospheric scintillation time series synthesizer based on stochastic differential equations," in *2013 Joint Conference: 19th Ka and Broadband Communications, Navigation and Earth Observation Conference and 31st AIAA ICSSC*, Oct. 2013.

[26] B. Beidas, R. Seshadri, and N. Becker, "Multicarrier successive predistortion for nonlinear satellite systems," *IEEE Trans. on Commun.*, vol. 63, no. 4, pp. 1373–1382, Apr. 2015.

[27] H. Meyr, M. Oerder, and A. Polydoros, "On sampling rate, analog prefiltering, and sufficient statistics for digital receivers," *IEEE Trans. on Commun.*, vol. 42, pp. 3208–3214, Dec. 1994.

[28] A. Ugolini, A. Modenini, G. Colavolpe, V. Mignone, and A. Morello, "Advanced techniques for spectrally efficient DVB-S2X systems," *Intern. J. of Satellite Communications and Networking*, article first published online: Sept. 2015.

[29] S. Verdú, *Multiuser Detection*. Cambridge, UK: Cambridge University Press, 1998.

[30] A. Modenini, F. Rusek, and G. Colavolpe, "Adaptive rate-maximizing channel-shortening for ISI channels," *IEEE Commun. Letters*, vol. 19, no. 12, pp. 2090–2093, Dec. 2015.

[31] D. M. Arnold, H.-A. Loeliger, P. O. Vontobel, A. Kavčić, and W. Zeng, "Simulation-based computation of information rates for channels with memory," *IEEE Trans. Inform. Theory*, vol. 52, no. 8, pp. 3498–3508, Aug. 2006.

[32] S. ten Brink, G. Kramer, and A. Ashikhmin, "Design of low-density parity-check codes for modulation and detection," *IEEE Trans. Commun.*, vol. 52, pp. 670–678, Apr. 2004.

[33] "AGI STK." [Online]. Available: https://www.agi.com/products/by-product-type/applications/stk/

[34] N. Lyras, C. Kourogiorgas, and A. D. Panagopoulos, "Joint statistics of cloud attenuation induced on multiple optical satellite links," in

21th Ka band and Broadband Communications, Navigation and Earth Observation Conference, Oct. 2015.